ACS OMEGA

http://pubs.acs.org/journal/acsodf

Article

Exploring the Optimal Alloy for Nitrogen Activation by Combining Bayesian Optimization with Density Functional Theory Calculations

Kazuki Okazawa, Yuta Tsuji, Keita Kurino, Masataka Yoshida, Yoshifumi Amamoto, and Kazunari Yoshizawa*

Cite This: *ACS Omega* 2022, 7, 45403−45408

Read Online

ACCESS | Metrics & More | Article Recommendations | Supporting Information

ABSTRACT: Binary alloy catalysts have the potential to exhibit higher activity than monometallic catalysts in nitrogen activation reactions. However, owing to the multiple possible combinations of metal elements constituting binary alloys, an exhaustive search for the optimal combination is difficult. In this study, we searched for the optimal binary alloy catalyst for nitrogen activation reactions using a combination of Bayesian optimization and density functional theory calculations. The optimal alloy catalyst proposed by Bayesian optimization had a surface energy of ∼0.2 eV/Å^2 and resulted in a low reaction heat for the dissociation of the N≡N bond. We demonstrated that the search for such binary alloy catalysts using Bayesian optimization is more efficient than random search.

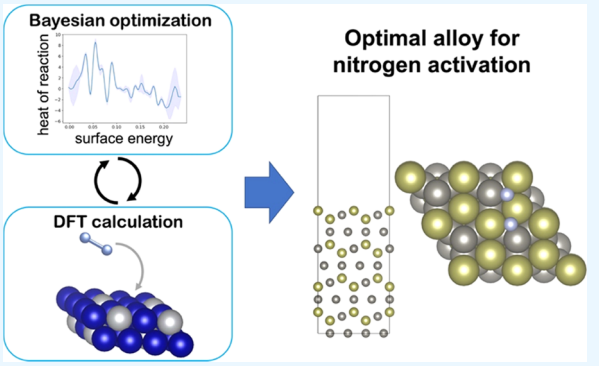

1. INTRODUCTION

Ammonia has emerged as an important hydrogen carrier and is also an important raw material for synthesizing nitrogen-containing compounds such as nitrogen fertilizers and chemicals.[1−3] Nitrogen fixation—the direct synthesis of ammonia from the abundant nitrogen gas in the atmosphere—is a very important process. However, since nitrogen is essentially an inert gas owing to its strong triple bond, a large amount of energy is required for its activation. The Haber−Bosch process is well known as the most efficient industrial method for synthesizing large quantities of ammonia.[4] This process synthesizes ammonia from nitrogen and hydrogen gases at very high temperatures (>400 °C) and pressures (>100 atm) using inexpensive iron-based catalysts. However, the process accounts for 1−2% of the annual global energy usage and burdens the environment considerably.[2,5] Therefore, it is necessary to develop a catalyst that can promote ammonia synthesis under milder conditions than those employed in the Haber−Bosch process. So far, homogeneous[6,7] and heterogeneous[8,9] catalysts have been investigated for ammonia synthesis.

The rate-determining step in the metal-catalyzed ammonia synthesis process is the dissociative adsorption of nitrogen molecules on the catalyst surface.[10−12] The triple bond of nitrogen is very strong and requires a very high bond dissociation energy (∼226 kcal/mol).[13] Ammonia synthesis requires high temperatures to induce the dissociative adsorption of nitrogen molecules. Therefore, ammonia synthesis under mild conditions necessitates the development of a catalyst that can activate nitrogen molecules at low temperatures.

Binary alloys have exhibited higher catalytic activity than pure metal catalysts and, consequently, have attracted considerable attention as catalysts.[14−20] Alloy catalysts that can promote methane activation[21] and CO hydrogenation[18] or control the selectivity of hydrogenation−dehydrogenation reactions[19] have been proposed before. Similarly, alloy catalysts that exhibit superior activity compared to iron-based catalysts have also been proposed.[14,15] Nitrogen activation should be achieved under milder conditions by optimizing the composition of alloy catalysts. However, since many combinations of metal elements constituting binary alloys are possible, it is difficult to conduct an exhaustive search for the optimal combination.

When the number of search targets is large, it is nearly impossible to perform an exhaustive search on a realistic time scale. To search for a target that satisfies the required conditions, efficient sampling must be ensured. Recently, Bayesian optimization (BO) has been revealed to be an efficient method for sampling from a huge number of search targets.[22] BO maximizes or minimizes an objective variable (function) based on some explanatory variables (descriptors).

Received: September 15, 2022
Accepted: November 9, 2022
Published: November 30, 2022

The optimal value is proposed based on an acquisition function, which is a function that takes into account the predicted value (mean) and predicted variance obtained by Gaussian process regression.[23,24] Various acquisition functions have been designed to propose globally optimal values by BO.[25] In materials science, BO is used to search for compositions and structures that can endow certain optimal physical properties.[26−31] Furthermore, BO is widely used in chemistry to optimize catalysts and synthetic conditions.[32−34] In recent years, not only BO but also various informatics methods have been introduced in the fields of catalysis and reactivity prediction.[35−39]

In this study, we explore the optimal catalyst for promoting the dissociation of the N≡N bond—the rate-determining step in ammonia synthesis, by combining BO and density functional theory (DFT)[40,41] calculations. Using three acquisition functions and by comparing the results of the three BOs and random sampling, we demonstrate that the search for alloy catalysts via the former is more efficient than that via the latter. To the best of our knowledge, this is the first study wherein BO and DFT calculations are combined to search for the best nitrogen activation alloy catalysts.

2. COMPUTATIONAL DETAILS

2.1. Acquisition of Alloy Structures. The structures of binary alloys used in this study were obtained from automatic-FLOW for materials discovery (AFLOW).[42] AFLOW is a database based on the results from calculations with the Vienna Ab initio Simulation Package (VASP).[43−46] The tool AFLOW-CHULL plots the relationship between composition and enthalpy of formation (convex hull diagram) for the alloys in the database. We added to the dataset the alloy crystal structures with negative enthalpies of formation, located at the bottom of the convex hull diagram. The dataset in this study consisted of 307 alloys and was identical to the dataset used in the previous study.[21]

2.2. DFT Calculations. *2.2.1. Surface Energy Calculations.* The crystal structures of the alloys obtained were cut along the (111), (110), (101), (011), (100), (010), (001), (11$\bar{1}$), (10$\bar{1}$), ($\bar{1}$11), ($\bar{1}$10), (01$\bar{1}$), and ($\bar{1}$11) planes, and slab models with alloy layers as thick as two repeating units and a 15 Å vacuum layer were created. The surface energy of each alloy was calculated with DFT using the created slab model. The surface energy of an alloy is defined as follows

$$\gamma = \frac{1}{2S}\left(E_{\mathrm{slab}} - \frac{n_{\mathrm{slab}}}{n_{\mathrm{bulk}}}E_{\mathrm{bulk}}\right) \quad (1)$$

Here, E_{slab} and E_{bulk} are the energies in the slab model and bulk state of the alloy, respectively; n_{slab} and n_{bulk} are the numbers of atoms in the slab and bulk models, respectively; and S is the area of the alloy surface in the slab model. We adopted the slab model with the lowest surface energy for each composition.

DFT calculations were performed using CASTEP as implemented in Materials Studio 16.1.[47] The Perdew−Burke−Ernzerhof (PBE) functional[48] and on-the-fly generated ultrasoft pseudopotential[49] were used. The cutoff energy of the plane-wave basis set was set to 400 eV, and the convergence condition for the self-consistent field (SCF) was set to 1.0×10^{-6} eV. The Brillouin zone was sampled with a spacing of $2\pi \times 0.05$ Å^{-1} using the Monkhorst−Pack method.[50] These surface energies were already calculated in our previous study.[21]

2.2.2. N−N Bond Dissociation on Alloy Surfaces. The slab models created for the adopted surfaces comprised a four-atom thick alloy layer and a 15 Å vacuum layer. Geometry optimization was performed with the fixed bottom two layers of each alloy slab model. Two nitrogen atoms were placed on the surface of the optimized slab, and geometry optimization was performed. All atoms except the nitrogen atoms were fixed. The reaction heat $\Delta_r H$ for N≡N bond cleavage is expressed by the following equation

$$\Delta_r H = E_{\mathrm{2N+slab}} - (E_{\mathrm{slab}} + E_{\mathrm{N_2}}) \quad (2)$$

Here, $E_{\mathrm{2N+slab}}$ is the energy of the slab model of the alloy with two nitrogen atoms, E_{slab} is the energy of the optimized slab model of the alloy, and $E_{\mathrm{N_2}}$ is the energy of the nitrogen molecule.

These calculations were performed using VASP. The PBE functional was used. The Kohn−Sham equation was solved by the projector-augmented wave method using a plane-wave basis set.[51] The cutoff energy of the plane-wave basis set was set to 500 eV, the convergence condition for SCF was set to 1.0×10^{-5} eV, and the convergence condition for structural optimization was set to 0.1 eV/Å. The Brillouin zone was sampled at intervals of $2\pi \times 0.05$ Å^{-1}.

2.3. Procedure for Bayesian Optimization. BO was performed on the dataset consisting of 307 stable alloy surfaces using PHYSBO.[52] The Gaussian kernel approximated by the random feature method was used as the kernel function for Gaussian process regression.[53] Hyperparameters were optimized by maximizing the Type II likelihood.[23] The surface energy at the most stable surface of the binary alloy and the reaction heat of N≡N bond cleavage were employed as explanatory and objective variables, respectively. As the initial data for performing BO, we used 30 data points obtained by equally spaced sampling from an alloy dataset sorted by surface energy. BO was performed using three different acquisition functions—the probability of improvement (PI),[54] expected improvement (EI),[55] and Thompson sampling (TS)—[56,57] for 20 cycles each. For comparison, 20 cycles of alloy search were performed by random sampling.

3. RESULTS AND DISCUSSION

3.1. Setting Explanatory and Objective Variables. The best catalyst for the promotion of nitrogen activation would be the one that lowers the activation barrier for the dissociation of the N≡N bond. However, calculation of the activation barrier involves a large computational cost. The Brønsted−Evans−Polanyi relationship suggests a linear relationship between the activation energy and heat of reaction for elementary reactions.[58] Therefore, the heat of reaction for N≡N bond cleavage, instead of the activation energy, was used as the objective variable in this study.

The reactions investigated in this study are surface reactions. Even for the same metal, surfaces with different facets have different catalytic activities.[59] Thus, in this study, it is inappropriate to employ parameters reflecting only bulk properties as explanatory variables. Moreover, to improve the performance of the BO, it is essential to choose explanatory variables that are closely related to the objective variable. Logadottir et al. reported that the adsorption energy of nitrogen atom on metal surfaces was linearly correlated to the activation energy for nitrogen dissociation when metal surfaces behaved as catalysts.[60] Furthermore, there was a positive

https://doi.org/10.1021/acsomega.2c05988
ACS Omega 2022, 7, 45403−45408

correlation between the adsorption energy and the surface energy of metals.[61] Consequently, there should be a correlation between the surface energy of metals and the activation energy for nitrogen dissociation. Hence, the surface energy was chosen as the explanatory variable.

3.2. Correlation of Initial Dataset. Figure 1 shows the relationship between the surface energy and heat of reaction for N≡N bond cleavage for the initial dataset. Details of the 30 data points in this plot are shown in the Supporting Information (SI). The correlation coefficient was −0.695, indicating a moderate negative correlation between the surface energy and heat of reaction for N≡N bond cleavage. This suggested that alloy catalysts with a large surface energy could reduce the heat of reaction for N≡N bond cleavage and that the search could be made more efficient by examining such catalysts. However, in this study, the alloy surface with the highest surface energy did not exhibit the lowest reaction heat for N≡N bond cleavage. Table 1 summarizes the five alloys that resulted in the lowest reaction heat for N≡N bond cleavage in the initial dataset. Fe_2Re_3, which has the highest surface energy in the explored dataset, leads to the fifth lowest heat of reaction for N≡N bond cleavage. The heats of reaction for N≡N bond cleavage on the surfaces of the ReV, $CoTa_2$, MnTa, and Cr_2Ti alloys were more than 0.8 eV lower than that on the surface of Fe_2Re_3. Hence, the surface energy and the reaction heat of N≡N bond cleavage do not have a simple linear correlation. To efficiently search for alloys that will allow N≡N bond cleavage at a low reaction heat, it is necessary to use BO based on Gaussian process regression, which can be extended to a nonlinear regression model by kernel tricks.[62]

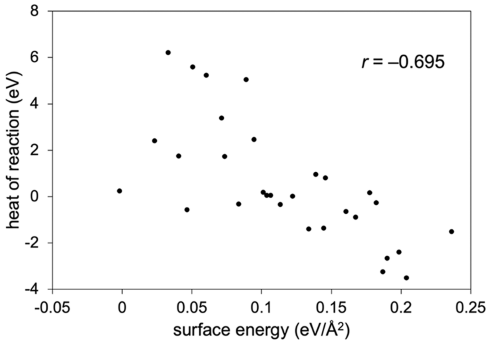

Figure 1. Scatter plot between the surface energy of alloys and the heat of reaction for N≡N bond cleavage in the initial dataset. *r* denotes the correlation coefficient.

Table 1. Five Lowest Reaction Heats for N≡N Bond Cleavage on the Alloys in the Initial Dataset and the Surface Energies of the Alloys

alloy	mirror index (*hkl*)	surface energy (eV/Å²)	heat of reaction (eV)
ReV	(110)	0.204	−3.499
$CoTa_2$	(101)	0.187	−3.235
MnTa	(110)	0.190	−2.647
Cr_2Ti	($\bar{1}$11)	0.199	−2.398
Fe_2Re_3	(110)	0.236	−1.512

3.3. Comparison of BO Using Each Acquisition Function and Random Search. Figure 2 shows the evolution of the minimum value of the objective variable in the BO and random search. The alloy-catalyzed heats of reaction for N≡N bond cleavage obtained in the three BO trials performed with each of the three different acquisition functions were lower than those obtained by the random search. The lowest heat of reaction for N≡N bond cleavage obtained after 20 optimization cycles is lower for PI, EI, and TS. The acquisition functions were developed based on two policies: exploitation and exploration. The acquisition function that emphasizes exploitation is used when the accuracy of prediction is important and optimization is efficient. On the other hand, an acquisition function that emphasizes exploration is used to acquire areas where data acquisition is inadequate. PI is a function that proposes a point with a high probability of updating the minimum value of the objective variable and is weighted toward exploitation.[63] Thus, BO with PI suggests a point near the current minimum of the objective variable. There is a negative correlation between the explanatory and objective variables in this study. Therefore, searching for alloys with lower reaction heats of N≡N bond cleavage in the initial dataset is expected to be the most efficient approach. In fact, BO with PI suggested the alloy with the surface energy closest to that of the alloy with the lowest reaction heat for N≡N bond cleavage in the initial dataset; indeed, the reaction heat for N≡N bond cleavage with that alloy was the lowest.

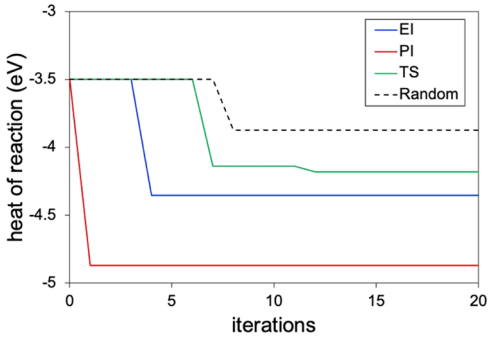

Figure 2. Convergence of the optimization of the heat of reaction for N≡N bond cleavage upon search by BO with EI, PI, and TS and upon random search.

We focused on the relationship between surface energy and heat of reaction for N≡N bond cleavage in the BO with PI; Table 2 summarizes the five alloys resulting in the lowest reaction heats of N≡N bond cleavage. The surface energies of all of the alloys listed in Table 2 are ∼0.2 eV/Å². The scatter plot of the relationship between the surface energy and reaction heat shows that alloys with surface energies of ∼0.2 eV/Å² exhibit low reaction heat for N≡N bond cleavage, whereas such is not the case for alloys with surface energies

Table 2. Alloys Conferring the Five Lowest Reaction Heats for the Dissociation of N≡N Bond, as Predicted by BO With PI

alloy	mirror index (*hkl*)	surface energy (eV/Å²)	heat of reaction (eV)
HfW_2	(111)	0.204	−4.87
Cr_2Ta	(111)	0.220	−4.35
VW_2	(110)	0.202	−4.18
TaW_2	(110)	0.201	−4.14
Cr_2V	(110)	0.203	−3.87

https://doi.org/10.1021/acsomega.2c05988
ACS Omega 2022, 7, 45403−45408

greater than 0.2 eV/Å^2 (Figure 3a). The alloys identified in the BO using EI also have surface energies of ∼0.2 eV/Å^2, except

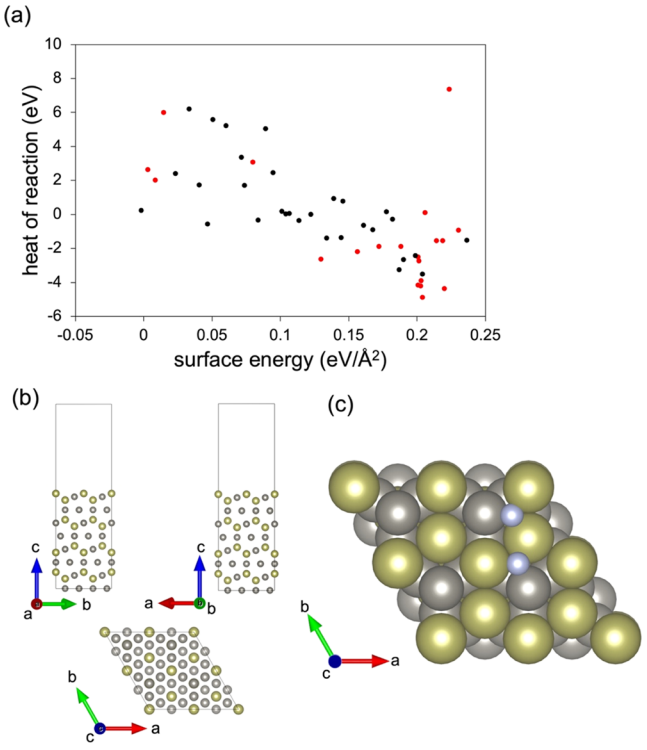

Figure 3. (a) Scatter plot between the surface energy and heat of reaction obtained after BO with PI (red dots), (b) structure of the slab model of the HfW_2(111) surface facet as seen from different angles, and (c) top view of the HfW_2(111) surface with two adsorbed N atoms. Black dots in (a) denote the initial datasets. Yellow, gray, and blue balls in (b) and (c) represent Hf, W, and N atoms, respectively. The structures were visualized by VESTA.[64]

for Tc_2Y (whose surface energy was 0.129 eV/Å^2), which has the fifth lowest reaction heat (Table S1). The BO using TS shows similar trends as those of BOs using PI and EI (Table S2). These trends indicate that alloy catalysts with surface energies of ∼0.2 eV/Å^2 are optimal for N≡N bond cleavage to proceed at a low reaction heat. Investigation of the electronic aspects of the relationship between the energetics of nitrogen cleavage and surface energies will be undertaken in future studies.

The alloy resulting in the lowest reaction heat for N≡N bond cleavage, as suggested by BO with PI, is HfW_2. Figure 3b,c shows the structure of the slab model of the HfW_2(111) surface and the structure of the 2N-adsorbed surface. The HfW_2 alloy could not be suggested by BO using EI or TS. Among the datasets used in this study, the surface energy of HfW_2 was the closest to that of ReV, which exhibits the lowest reaction heat in the initial dataset. Therefore, HfW_2 was proposed owing to the weight of exploitation in PI.

4. CONCLUSIONS

BO was combined with DFT calculations to explore optimal alloy catalysts for the dissociative adsorption of nitrogen molecule, which is the rate-determining step in ammonia synthesis reactions. The correlation coefficient between the explanatory variable, i.e., the surface energy of the alloy, and the objective variable, i.e., the heat of reaction for the dissociation of the N≡N bond, for the initial dataset was −0.695, suggesting a negative linear correlation between surface energy and heat of reaction. The heats of reaction obtained by BO with the three acquisition functions were lower than that obtained by the random search, suggesting higher efficiency of the former approach. Furthermore, the alloys resulting in low heats of reaction, as proposed by BO, had surface energies of ∼0.2 eV/Å^2. In contrast, alloys with surface energies larger than 0.2 eV/Å^2 exhibit higher reaction heat for N≡N bond cleavage. Therefore, an alloy surface with a surface energy of 0.2 eV/Å^2 was an optimal alloy catalyst for promoting the dissociation of the N≡N bond. This study has demonstrated the possibility of combining Bayesian optimization and DFT calculations to efficiently search for the best catalyst to promote nitrogen activation among a vast number of alloys, significant as a model case where data science and computational chemistry work hand in hand to challenge catalyst research. In future, we plan to propose an optimal alloy catalyst for ammonia synthesis by performing multiobjective BO using the heats of reaction for the dissociation of the N≡N bond and desorption of ammonia as the objective variables.

■ ASSOCIATED CONTENT

Supporting Information

The Supporting Information is available free of charge at https://pubs.acs.org/doi/10.1021/acsomega.2c05988.

Surface energies of 307 alloys, surface energies and heats of reaction for the initial dataset, and alloys resulting in the five lowest reaction heats for the dissociation of the N≡N bond, as obtained after BO using EI and TS (PDF)

■ AUTHOR INFORMATION

Corresponding Author

Kazunari Yoshizawa − *Institute for Materials Chemistry and Engineering and IRCCS, Kyushu University, Fukuoka 819-0395, Japan;* orcid.org/0000-0002-6279-9722; Email: kazunari@ms.ifoc.kyushu-u.ac.jp

Authors

Kazuki Okazawa − *Institute for Materials Chemistry and Engineering and IRCCS, Kyushu University, Fukuoka 819-0395, Japan;* orcid.org/0000-0001-6515-4367

Yuta Tsuji − *Faculty of Engineering Sciences, Kyushu University, Fukuoka 816-8580, Japan;* orcid.org/0000-0003-4224-4532

Keita Kurino − *Institute for Materials Chemistry and Engineering and IRCCS, Kyushu University, Fukuoka 819-0395, Japan*

Masataka Yoshida − *Laboratory for Chemistry and Life Science, Tokyo Institute of Technology, Yokohama 226-8503, Japan*

Yoshifumi Amamoto − *Institute for Materials Chemistry and Engineering and IRCCS, Kyushu University, Fukuoka 819-0395, Japan*

Complete contact information is available at: https://pubs.acs.org/10.1021/acsomega.2c05988

Notes

The authors declare no competing financial interest.

https://doi.org/10.1021/acsomega.2c05988
ACS Omega 2022, 7, 45403−45408

■ ACKNOWLEDGMENTS

This work was supported by KAKENHI grants (number JP21K04996 and JP22H00335) from the Japan Society for the Promotion of Science (JSPS) and the Ministry of Education, Culture, Sports, Science and Technology of Japan (MEXT) through the MEXT projects Integrated Research Consortium on Chemical Sciences, Cooperative Research Program of Network Joint Research Center for Materials and Devices and Elements Strategy Initiative to Form Core Research Center, and by JST-CREST JPMJCR15P5, JST-Mirai JPMJMI18A2, and JST, the establishment of university fellowships toward the creation of science technology innovation JPMJFS2132. The authors are grateful for a JSPS Grant-in-Aid for Scientific Research on Innovative Areas (Discrete Geometric Analysis for Materials Design, grant number JP20H04643, and Mixed Anion, grant number JP19H04700) and a Grant-in-Aid for Transformative Research Areas (A) "Supra-ceramics" (grant number JP22H05146). Y.T. acknowledges JACI Prize for Encouraging Young Researcher. This article is also based on results obtained from a project, JPNP21020, commissioned by the New Energy and Industrial Technology Development Organization (NEDO). The computations in this work were primarily performed using the computer facilities at the Research Institute for Information Technology, Kyushu University.

■ REFERENCES

(1) Smil, V. Detonator of the Population Explosion. *Nature* **1999**, *400*, No. 415.
(2) Erisman, J. W.; Sutton, M. A.; Galloway, J.; Klimont, Z.; Winiwarter, W. How a Century of Ammonia Synthesis Changed the World. *Nat. Geosci.* **2008**, *1*, 636−639.
(3) Klerke, A.; Christensen, C. H.; Nørskov, J. K.; Vegge, T. Ammonia for Hydrogen Storage: Challenges and Opportunities. *J. Mater. Chem.* **2008**, *18*, 2304.
(4) Liu, H. Ammonia Synthesis Catalyst 100 Years: Practice, Enlightenment and Challenge. *Chin. J. Catal.* **2014**, *35*, 1619−1640.
(5) Kyriakou, V.; Garagounis, I.; Vourros, A.; Vasileiou, E.; Stoukides, M. An Electrochemical Haber-Bosch Process. *Joule* **2020**, *4*, 142−158.
(6) Yandulov, D. V.; Schrock, R. R. Catalytic Reduction of Dinitrogen to Ammonia at a Single Molybdenum Center. *Science* **2003**, *301*, 76−78.
(7) Ashida, Y.; Arashiba, K.; Nakajima, K.; Nishibayashi, Y. Molybdenum-Catalysed Ammonia Production with Samarium Diiodide and Alcohols or Water. *Nature* **2019**, *568*, 536−540.
(8) Kobayashi, Y.; Tang, Y.; Kageyama, T.; Yamashita, H.; Masuda, N.; Hosokawa, S.; Kageyama, H. Titanium-Based Hydrides as Heterogeneous Catalysts for Ammonia Synthesis. *J. Am. Chem. Soc.* **2017**, *139*, 18240−18246.
(9) Tsuji, Y.; Okazawa, K.; Kobayashi, Y.; Kageyama, H.; Yoshizawa, K. Electronic Origin of Catalytic Activity of TiH_2 for Ammonia Synthesis. *J. Phys. Chem. C* **2021**, *125*, 3948−3960.
(10) Vojvodic, A.; Medford, A. J.; Studt, F.; Abild-Pedersen, F.; Khan, T. S.; Bligaard, T.; Nørskov, J. K. Exploring the Limits: A Low-Pressure, Low-Temperature Haber−Bosch Process. *Chem. Phys. Lett.* **2014**, *598*, 108−112.
(11) Housecroft, C. E.; Sharpe, A. G.*Inorganic Chemistry*, 3rd ed.; Pearson Education: Harlow, 2008; Vol. *1*.
(12) Ertl, G. Surface Science and Catalysis—Studies on the Mechanism of Ammonia Synthesis: The P. H. Emmett Award Address. *Catal. Rev.* **1980**, *21*, 201−223.
(13) Gambarotta, S.; Scott, J. Multimetallic Cooperative Activation of N2. *Angew. Chem., Int. Ed.* **2004**, *43*, 5298−5308.
(14) Jacobsen, C. J. H. Novel Class of Ammonia Synthesis Catalysts. *Chem. Commun.* **2000**, *12*, 1057−1058.
(15) Rai, R. K.; Al Maksoud, W.; Morlanés, N.; Harb, M.; Ahmad, R.; Genovese, A.; Hedhili, M. N.; Cavallo, L.; Basset, J.-M. Iron−Cobalt-Based Materials: An Efficient Bimetallic Catalyst for Ammonia Synthesis at Low Temperatures. *ACS Catal.* **2022**, *12*, 587−599.
(16) Shinzato, K.; Tagawa, K.; Tsunematsu, K.; Gi, H.; Singh, P. K.; Ichikawa, T.; Miyaoka, H. Systematic Study on Nitrogen Dissociation and Ammonia Synthesis by Lithium and Group 14 Element Alloys. *ACS Appl. Energy Mater.* **2022**, *5*, 4765−4773.
(17) Tao, F.; Zhang, S.; Nguyen, L.; Zhang, X. Action of Bimetallic Nanocatalysts under Reaction Conditions and during Catalysis: Evolution of Chemistry from High Vacuum Conditions to Reaction Conditions. *Chem. Soc. Rev.* **2012**, *41*, 7980.
(18) Klötzer, B.; Unterberger, W.; Hayek, K. Adsorption and Hydrogenation of CO on Pd(1 1 1) and Rh(1 1 1) Modified by Subsurface Vanadium. *Surf. Sci.* **2003**, *532*−*535*, 142−147.
(19) Hwu, H. H.; Eng, J.; Chen, J. G. Ni/Pt(111) Bimetallic Surfaces: Unique Chemistry at Monolayer Ni Coverage. *J. Am. Chem. Soc.* **2002**, *124*, 702−709.
(20) Kyriakou, G.; Boucher, M. B.; Jewell, A. D.; Lewis, E. A.; Lawton, T. J.; Baber, A. E.; Tierney, H. L.; Flytzani-Stephanopoulos, M.; Sykes, E. C. H. Isolated Metal Atom Geometries as a Strategy for Selective Heterogeneous Hydrogenations. *Science* **2012**, *335*, 1209−1212.
(21) Yoshida, M.; Tsuji, Y.; Iguchi, S.; Nishiguchi, H.; Yamanaka, I.; Abe, H.; Kamachi, T.; Yoshizawa, K. Toward Computational Screening of Bimetallic Alloys for Methane Activation: A Case Study of MgPt Alloy. *ACS Catal.* **2022**, *12*, 9458−9472.
(22) Terayama, K.; Sumita, M.; Tamura, R.; Tsuda, K. Black-Box Optimization for Automated Discovery. *Acc. Chem. Res.* **2021**, *54*, 1334−1346.
(23) Rasmussen, C. E.; Williams, C. K. I.*Gaussian Processes for Machine Learning*; The MIT Press, 2005. DOI: 10.7551/mitpress/3206.001.0001.
(24) Varnek, A.; Baskin, I. Machine Learning Methods for Property Prediction in Chemoinformatics: Quo Vadis? *J. Chem. Inf. Model.* **2012**, *52*, 1413−1437.
(25) Shahriari, B.; Swersky, K.; Wang, Z.; Adams, R. P.; de Freitas, N. Taking the Human Out of the Loop: A Review of Bayesian Optimization. *Proc. IEEE* **2016**, *104*, 148−175.
(26) Ju, S.; Shiga, T.; Feng, L.; Hou, Z.; Tsuda, K.; Shiomi, J. Designing Nanostructures for Phonon Transport via Bayesian Optimization. *Phys. Rev. X* **2017**, *7*, No. 021024.
(27) Balachandran, P. V.; Kowalski, B.; Sehirlioglu, A.; Lookman, T. Experimental Search for High-Temperature Ferroelectric Perovskites Guided by Two-Step Machine Learning. *Nat. Commun.* **2018**, *9*, No. 1668.
(28) Kikuchi, S.; Oda, H.; Kiyohara, S.; Mizoguchi, T. Bayesian Optimization for Efficient Determination of Metal Oxide Grain Boundary Structures. *Phys. B: Condens. Matter* **2018**, *532*, 24−28.
(29) Fukazawa, T.; Harashima, Y.; Hou, Z.; Miyake, T. Bayesian Optimization of Chemical Composition: A Comprehensive Framework and Its Application to RFe12-Type Magnet Compounds. *Phys. Rev. Mater.* **2019**, *3*, No. 053807.
(30) Hashimoto, W.; Tsuji, Y.; Yoshizawa, K. Optimization of Work Function via Bayesian Machine Learning Combined with First-Principles Calculation. *J. Phys. Chem. C* **2020**, *124*, 9958−9970.
(31) Hughes, Z. E.; Nguyen, M. A.; Wang, J.; Liu, Y.; Swihart, M. T.; Poloczek, M.; Frazier, P. I.; Knecht, M. R.; Walsh, T. R. Tuning Materials-Binding Peptide Sequences toward Gold- and Silver-Binding Selectivity with Bayesian Optimization. *ACS Nano* **2021**, *15*, 18260−18269.
(32) Nugraha, A. S.; Lambard, G.; Na, J.; Hossain, M. S. A.; Asahi, T.; Chaikittisilp, W.; Yamauchi, Y. Mesoporous Trimetallic PtPdAu Alloy Films toward Enhanced Electrocatalytic Activity in Methanol Oxidation: Unexpected Chemical Compositions Discovered by Bayesian Optimization. *J. Mater. Chem. A* **2020**, *8*, 13532−13540.
(33) Pedersen, J. K.; Clausen, C. M.; Krysiak, O. A.; Xiao, B.; Batchelor, T. A. A.; Löffler, T.; Mints, V. A.; Banko, L.; Arenz, M.; Savan, A.; Schuhmann, W.; Ludwig, A.; Rossmeisl, J. Bayesian

https://doi.org/10.1021/acsomega.2c05988
ACS Omega 2022, 7, 45403−45408

Optimization of High-Entropy Alloy Compositions for Electrocatalytic Oxygen Reduction. *Angew. Chem., Int. Ed.* **2021**, *60*, 24144−24152.
(34) Shields, B. J.; Stevens, J.; Li, J.; Parasram, M.; Damani, F.; Alvarado, J. I. M.; Janey, J. M.; Adams, R. P.; Doyle, A. G. Bayesian Reaction Optimization as a Tool for Chemical Synthesis. *Nature* **2021**, *590*, 89−96.
(35) Takahashi, K.; Takahashi, L.; Miyazato, I.; Fujima, J.; Tanaka, Y.; Uno, T.; Satoh, H.; Ohno, K.; Nishida, M.; Hirai, K.; Ohyama, J.; Nguyen, T. N.; Nishimura, S.; Taniike, T. The Rise of Catalyst Informatics: Towards Catalyst Genomics. *ChemCatChem* **2019**, *11*, 1146−1152.
(36) Toyao, T.; Maeno, Z.; Takakusagi, S.; Kamachi, T.; Takigawa, I.; Shimizu, K. I. Machine Learning for Catalysis Informatics: Recent Applications and Prospects. *ACS Catal.* **2020**, *10*, 2260−2297.
(37) Muratov, E. N.; Bajorath, J.; Sheridan, R. P.; Tetko, I. V.; Filimonov, D.; Poroikov, V.; Oprea, T. I.; Baskin, I. I.; Varnek, A.; Roitberg, A.; Isayev, O.; Curtalolo, S.; Fourches, D.; Cohen, Y.; Aspuru-Guzik, A.; Winkler, D. A.; Agrafiotis, D.; Cherkasov, A.; Tropsha, A. QSAR without Borders. *Chem. Soc. Rev.* **2020**, *49*, 3525−3564.
(38) Afonina, V. A.; Mazitov, D. A.; Nurmukhametova, A.; Shevelev, M. D.; Khasanova, D. A.; Nugmanov, R. I.; Burilov, V. A.; Madzhidov, T. I.; Varnek, A. Prediction of Optimal Conditions of Hydrogenation Reaction Using the Likelihood Ranking Approach. *Int. J. Mol. Sci.* **2022**, *23*, 248.
(39) Stuyver, T.; Coley, C. W. Quantum Chemistry-Augmented Neural Networks for Reactivity Prediction: Performance, Generalizability, and Explainability. *J. Chem. Phys.* **2022**, *156*, No. 084104.
(40) Hohenberg, P.; Kohn, W. Inhomogeneous Electron Gas. *Phys. Rev.* **1964**, *136*, B864−B871.
(41) Kohn, W.; Sham, L. J. Self-Consistent Equations Including Exchange and Correlation Effects. *Phys. Rev.* **1965**, *140*, A1133−A1138.
(42) Curtarolo, S.; Setyawan, W.; Hart, G. L. W.; Jahnatek, M.; Chepulskii, R. V.; Taylor, R. H.; Wang, S.; Xue, J.; Yang, K.; Levy, O.; Mehl, M. J.; Stokes, H. T.; Demchenko, D. O.; Morgan, D. AFLOW: An Automatic Framework for High-Throughput Materials Discovery. *Comput. Mater. Sci.* **2012**, *58*, 218−226.
(43) Kresse, G.; Hafner, J. Ab Initio Molecular Dynamics for Liquid Metals. *Phys. Rev. B* **1993**, *47*, 558−561.
(44) Kresse, G.; Hafner, J. Ab Initio Molecular-Dynamics Simulation of the Liquid-Metal−Amorphous-Semiconductor Transition in Germanium. *Phys. Rev. B* **1994**, *49*, 14251−14269.
(45) Kresse, G.; Furthmüller, J. Efficiency of Ab-Initio Total Energy Calculations for Metals and Semiconductors Using a Plane-Wave Basis Set. *Comput. Mater. Sci.* **1996**, *6*, 15−50.
(46) Kresse, G.; Joubert, D. From Ultrasoft Pseudopotentials to the Projector Augmented-Wave Method. *Phys. Rev. B* **1999**, *59*, 1758−1775.
(47) Clark, S. J.; Segall, M. D.; Pickard, C. J.; Hasnip, P. J.; Probert, M. I. J.; Refson, K.; Payne, M. C. First Principles Methods Using CASTEP. *Z. Kristallogr. - Cryst. Mater.* **2005**, *220*, 567−570.
(48) Perdew, J. P.; Burke, K.; Ernzerhof, M. Generalized Gradient Approximation Made Simple. *Phys. Rev. Lett.* **1996**, *77*, 3865−3868.
(49) Vanderbilt, D. Soft Self-Consistent Pseudopotentials in a Generalized Eigenvalue Formalism. *Phys. Rev. B* **1990**, *41*, 7892−7895.
(50) Monkhorst, H. J.; Pack, J. D. Special Points for Brillouin-Zone Integrations. *Phys. Rev. B* **1976**, *13*, 5188−5192.
(51) Blöchl, P. E. Projector Augmented-Wave Method. *Phys. Rev. B* **1994**, *50*, 17953−17979.
(52) Motoyama, Y.; Tamura, R.; Yoshimi, K.; Terayama, K.; Ueno, T.; Tsuda, K. Bayesian Optimization Package: PHYSBO. *Comput. Phys. Commun.* **2022**, *278*, No. 108405.
(53) Rahimi, A.; Recht, B. In *Random Features for Large-Scale Kernel Machines*, Proceedings of the 20th International Conference on Neural Information Processing Systems; NIPS'07; Curran Associates Inc.: Red Hook, NY, USA, 2007; pp 1177−1184.
(54) Seko, A.; Maekawa, T.; Tsuda, K.; Tanaka, I. Machine Learning with Systematic Density-Functional Theory Calculations: Application to Melting Temperatures of Single- and Binary-Component Solids. *Phys. Rev. B* **2014**, *89*, No. 054303.
(55) Jones, D. R.; Schonlau, M.; Welch, W. J. Efficient Global Optimization of Expensive Black-Box Functions. *J. Glob. Optim.* **1998**, *13*, 455−492.
(56) Chapelle, O.; Li, L. In *An Empirical Evaluation of Thompson Sampling*, Adv. Neural Inf. Process. Syst. 24 25th Annu. Conf. Neural Inf. Process. Syst., NIPS, 2011.
(57) Russo, D. J.; Van Roy, B.; Kazerouni, A.; Osband, I.; Wen, Z.A Tutorial on Thompson Sampling. In *Foundations and Trends in Machine Learning*; Now Publishers, Inc., 2018; pp 1−96.
(58) Evans, M. G.; Polanyi, M. Inertia and Driving Force of Chemical Reactions. *Trans. Faraday Soc.* **1938**, *34*, 11.
(59) Spencer, N. D.; Schoonmaker, R. C.; Somorjai, G. A. Iron Single Crystals as Ammonia Synthesis Catalysts: Effect of Surface Structure on Catalyst Activity. *J. Catal.* **1982**, *74*, 129−135.
(60) Logadottir, A.; Rod, T. H.; Nørskov, J. K.; Hammer, B.; Dahl, S.; Jacobsen, C. J. H. The Brønsted−Evans−Polanyi Relation and the Volcano Plot for Ammonia Synthesis over Transition Metal Catalysts. *J. Catal.* **2001**, *197*, 229−231.
(61) Li, S. J.; Zhou, Y. T.; Kang, X.; Liu, D. X.; Gu, L.; Zhang, Q. H.; Yan, J. M.; Jiang, Q. A Simple and Effective Principle for a Rational Design of Heterogeneous Catalysts for Dehydrogenation of Formic Acid. *Adv. Mater.* **2019**, *31*, No. 1806781.
(62) Xiao, Z.; Zhan, S.; Xiang, Z.; Wang, D.; Chen, W. In *A GPR-PSO Incremental Regression Framework on GPS/INS Integration for Vehicle Localization under Urban Environment*, 2016 IEEE 27th Annual International Symposium on Personal, Indoor, And Mobile Radio Communications (PIMRC), IEEE, 2016.
(63) Wang, H.; Emmerich, M.; Van Stein, B.; Bäck, T. In *A New Acquisition Function for Bayesian Optimization Based on the Moment-Generating Function*, 2017 IEEE International Conference on Systems, Man, and Cybernetics (SMC), IEEE, 2017; pp 507−512.
(64) Momma, K.; Izumi, F. VESTA 3 for Three-Dimensional Visualization of Crystal, Volumetric and Morphology Data. *J. Appl. Crystallogr.* **2011**, *44*, 1272−1276.

https://doi.org/10.1021/acsomega.2c05988
ACS Omega 2022, 7, 45403−45408